Rearrangements of 2-Nitrobenzyl Compounds. 2. Substituent Effects on the Reactions of the Quinonoid Intermediates

Yuri V. Il'ichev*

Department of Chemistry, Wichita State University, 1845 Fairmount, Wichita, Kansas 67260-0051

Received: June 16, 2003; In Final Form: September 11, 2003

Photoinduced tautomerization of 2-nitrobenzyl derivatives (**1**) gives rise to quinonoid intermediates (**2**), which may undergo further reactions competing with the retautomerization to **1**. Rearrangements of **2** with different α substituents were studied with methods based on the density functional theory. The B3LYP functional with three different basis sets was used to optimize geometries of the minimum-energy and transition structures. The single-point energies were computed at these geometries by using the 6-311+G(2d,p) basis set in combination with four different hybrid functionals. Bulk solvent effects were estimated from the B3LYP/6-311+G(2d,p) free energies computed at the gas-phase geometries with the self-consistent reaction field polarized continuum model method. A common reaction pathway for the *E* isomers of substituted **2** was identified as the exothermic cyclization leading to 2,1-benzoxazoline derivatives (**3**). The cyclization was predicted to be highly stereoselective, two distinct modes of the reaction were found for two stereoisomers differing in the position of the α substituent relative to the nitronic moiety. The activation barrier for the cyclization appeared to be reasonably well correlated with the electron-donating ability of the substituent that was characterized by the Hammett-type σ_p^+ constants. The effective barrier height for the tautomerization **2** → **1** showed an opposite trend. The isomerization **2** → **3** was predicted to compete efficiently with retautomerization for all compounds except for the parent compound and those with strong electron-withdrawing susbstituents. The cyclization of **2** in the gas phase and water was predicted to encounter a much smaller activation barrier than the analogous isomerization reaction of the deprotonated species (**2**$^-$). Very high activation energies for the reaction **2**$^-$ → **3**$^-$ were linked to profound structural changes predicted for deprotonation of **3**. The computational results were discussed in respect to mechanism(s) of the photoinduced isomerization of **1** and to development of more efficient photolabile protecting groups.

Introduction

The 2-nitrobenzyl group has gained wide acceptance as a photolabile protector in organic synthesis,[1−5] polymer chemistry,[6] microelectronics,[7] and biomedical applications.[8−16] Photoinduced decomposition of 2-nitrobenzyl derivatives (**1** in Scheme 1) is initiated by fast tautomerization that affords quinonoid intermediates (**2**, also known as nitronic acids or *aci*-forms). The mechanism shown in Scheme 1 has recently been proposed on the basis of computational[17] and experimental studies[10,18,19] of model compounds. According to this mechanism, release of a protected substrate (X) is brought about by a sequence of essentially irreversible reactions of the protonated species (**2**−**4**) and the release rate does not necessarily coincide with the easily measured rate of the *aci*-form decay. In our DFT study[17] of the ground-state potential energy surface of 2-nitrotoluene (**1a**, X = H), we have been able to identify three pathways for concerted rearrangements of the neutral species in the gas phase, all of them involved **2a** and a bicyclic intermediate (**3a**). The two slowest steps in the lowest-energy pathway have been found to be 1,3-hydrogen shifts in **2a** and **3a**. The activation barrier for this reaction in **2a** has been predicted to be substantially higher than that for retautomerization **2a** → **1a**. This result is in agreement with experimental observation of the reversible (photochromic) reaction of **1a**, i.e., very low quantum yields of formation of **4a**.[10,20] Deprotonation

SCHEME 1. Mechanism of Photoinduced Isomerization of 2-Nitrobenzyl Derivatives

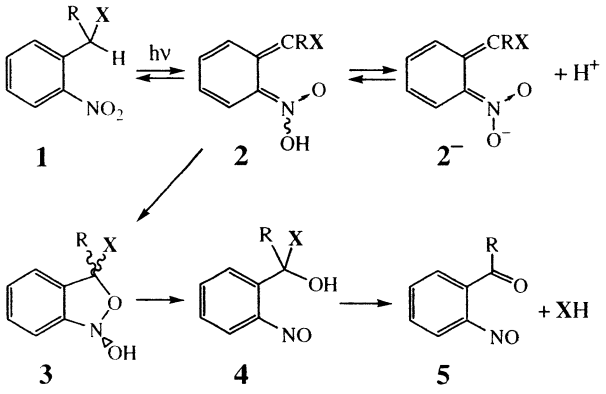

of moderately strong acids **2** readily occurs in polar solvents.[10,12,21] Reactivity of anionic species obtained by deprotonation of **1a**−**4a** has also been explored in our computational study.[17] A single isomerization pathway located for the common anion (**2a**$^-$) of **1a** and **2a** in the gas phase has been characterized as an endothermic reaction with an activation barrier more than twice as large as that for the energetically favorable cyclization of the protonated form. There also exists a growing body of experimental evidence showing that the cyclization of quinonoid intermediates of 2-nitrobenzyl derivatives proceeds almost exclusively through the protonated form of **2**.[10,18,19,21] The

* Tel: 316-978-5702. Fax: 316-978-3431. E-mail: Yuri.Ilitchev@wichita.edu.

10.1021/jp0357121 CCC: $25.00
Published on Web 11/05/2003

SCHEME 2. Cyclization Reactions and the Atom Numbering Scheme for the Two Stereoisomers of 2

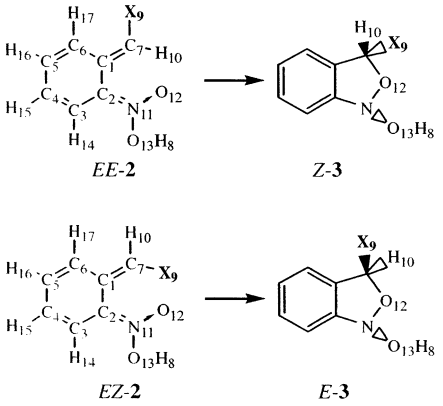

X = H (**a**), CH_3 (**b**), CN (**c**), F (**d**), Cl (**e**), NH_2 (**f**), NHCHO (**g**), NH_3^+ (**h**), OH (**i**), OCH_3 (**j**), OCHO (**k**)

mechanism shown in Scheme 1 is contrasted with that proposed earlier from studies of 2-nitrobenzyl phosphate esters in aqueous solutions.[12,13] The latter mechanism has suggested the deprotonated form of **2** as a key intermediate undergoing the fast cyclization in aqueous solution. However, this mechanism failed to explain the acid catalysis observed for various derivatives without extra groups that could be protonated. Further support for the mechanism of Scheme 1 has recently been obtained in a study of β-substituted 2-nitrophenylethyl derivatives.[22]

For practical applications, high quantum yields of the photoinduced isomerization of 2-nitrobenzyl derivatives and high release rates are greatly advantageous. Both parameters were found to vary considerably with substitution pattern and reaction medium.[10,12,14,16,21,23−26] An illustrative example is provided by the photoreaction of 4,5-dimethoxy-2-nitrobenzylamine in aqueous solution. The photoisomerization quantum yield was reduced by about 2 orders of magnitude in acidic solutions with a pH below the pK_a of the amino group.[24] A similar effect on the quantum yield was observed when three methoxy groups were introduced into the benzene ring of highly reactive 2-nitrobenzyl alcohol (X = OH, **2i**).[23a] The photodecomposition yields for derivatives of **2i** and 2-nitrobenzylamine (X = NH_2, **2f**) were found to strongly decrease upon acetylation of the α substituent. In the literature, the rate of the end product formation (protected group release) is often taken to be equal to the decay rate for **2**. The latter was found to vary by several orders of magnitude depending on the nitro compound and experimental conditions.[10,12,13,18−21] Moreover, recent data indicate that the rate of the *aci*-form decay may strongly differ from that for the formation of the final products.

Substituent effects on the photoisomerization efficiency and kinetics of the decay of quinonoid intermediates remain poorly understood. To gain better understanding of structural and electronic factors governing the isomerization reactions of **2**, we have undertaken a computational study of several model compounds with different α substituents (see Scheme 2). When we decided on the substituents for this study, preference was given to compounds modeling the nitrobenzyl derivatives of practical importance, such as esters and amides. The key reaction steps were identified by exploring the potential energy surface for the parent compound **2a** and several derivatives both in water and in the gas phase. Reaction energies and activation barriers for the cyclization and tautomerization of **2** were determined by using DFT-based methods. The isomerization reaction was also explored for the deprotonated species ($\mathbf{2}^-$). The results obtained strongly supported the reaction mechanism shown in Scheme 1. The data also provided a rationale for interpretation of experimental results and for optimization of the photolabile protecting groups based on 2-nitrobenzyl chemistry.

Computational Methods

All calculations were performed with the Gaussian 98 package of programs.[27] Geometries of the neutral molecules were fully optimized at the B3LYP/6-31G(d) level of theory which has been shown to provide good-quality parameters for **1a**.[17] The 6-31+G(d) basis set was used for anions. It is known that basis sets augmented with diffuse functions on the heavy atoms provide better results for anionic species.[28] Complexes of 2-nitrotoluene isomers with a water molecule were optimized at the B3LYP/6-31G(d,p) level. Single-point energies for the geometries were computed by using the B3LYP, B3PW91, B1LYP, and BHLYP hybrid functional with the 6-311+G(2d,p) basis set. B3LYP and B3PW91 are combinations of Becke's three-parameter exchange functional[29] with the slightly modified Lee−Yang−Parr (LYP)[30] and Perdew−Wang (PW91)[31] correlation functionals, respectively. B1LYP denotes Becke's one-parameter hybrid functional with the LYP correlation functional as implemented by Adamo and Barone.[32] BHLYP is the half-and-half functional in the form implemented in Gaussian 98, which is different from the functional initially proposed by Becke.[33]

Self-consistent reaction field (SCRF) calculations were performed to estimate solvent effects on activation barriers and reaction energies. The polarized continuum model (PCM) of Tomasi and co-workers[34] with water (ϵ = 78.4) as a solvent was used. The scaling factor for solvent-accessible surfaces and the initial number of tesserae on the surface of each sphere were set to default values of 1.2 and 60, respectively.

Transition structures (TS) on the potential energy surface were located by using the facility of Gaussian for the synchronous transit-guided quasi-Newton method.[35] Reaction pathways were computed for the rearrangements of several derivatives (**2a**, **2i**, **2j**) and their anions to verify the connection of TS to the local minima. The intrinsic reaction coordinate (IRC) method[36] was used to trace the steepest descent paths toward the reactants and the products. A normal vibrational mode corresponding to the single imaginary frequency was inspected to provide similar verification for other compounds. For all stationary points, the wave function stability was tested and harmonic vibrational frequencies were calculated using analytical second derivatives.

Results

Potential Energy Profile for 2-Nitrotoluene in the Gas Phase and in Water. In our previous computational study,[17] we have identified 1,3-hydrogen shifts in **2a** and **3a** as kinetic "bottlenecks" for the photoinduced isomerization of **1a** into 2-nitrosobenzyl alcohol (**4a**) in the gas phase. However, substantial reduction of the activation energy is expected for reactions of this type in protic solvents. Figure 1 shows schematic potential energy profiles for the reaction **2a** → **4a** in the gas phase and in water. This profile for the gas phase was constructed by using the B3LYP/6-311+G(2d,p)//B3LYP/6-31G(d,p) energies corrected to the scaled zero-point vibrational energies. Geometries of hydrogen-bonded complexes with a single water molecule were optimized at the B3LYP/6-31G-(d,p) level in the gas phase and henceforth were used to estimate total free energies in water with the SCRF-PCM method at the

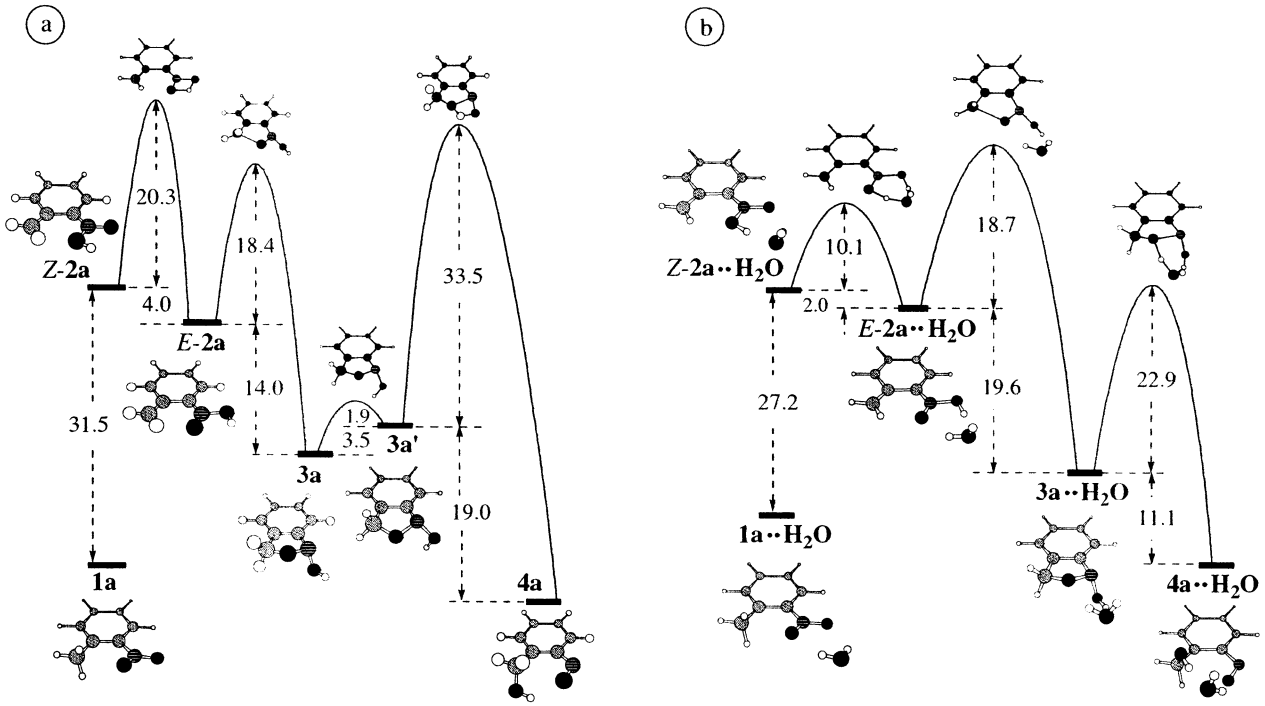

Figure 1. Schematic potential energy profiles for the isomerization of 2-nitrotoluene (**1**) in the gas-phase (a) and in water (b). Geometries were optimized in the gas phase at the B3LYP/6-31G(d,p) level of theory. The B3LYP/6-311+G(2d,p) single-point energies that were computed at these geometries and corrected to the zero-point vibrational energies (sZPE) scaled by 0.9806 were used to calculate the relative energies. The B3LYP method in combination with the 6-311++G(2d,2p) basis set and the SCRF-PCM model was utilized to estimate the relative free energies in water. All values are given in kcal mol^{-1}. The white circles represent H atoms; the gray circles, C atoms; the black circles, O atoms; and the circles with black horizontal lines, N atoms.

B3LYP/6-311++G(2d,2p) level of theory. The activation barriers were found to decrease by 10.2 and 10.6 kcal mol^{-1} for solvent-assisted proton-transfer reactions in **2a** and **3a**, respectively. In contrast, practically the same barrier height was predicted for the cyclization of *E*-**2a** in the gas phase and in water. Identical values of the activation free energy were obtained when the PCM method was applied to *E*-**2a** and its complex with H_2O. The highest-energy transition structure on the pathway from **2a** to **4a** in water was that for the *aci*-form cyclization. In aqueous solution, additional stabilization by 3−6 kcal mol^{-1} was predicted for the quinonoid intermediates (**2a**) and the bicyclic intermediate (**3a**). The rearrangement **3a** → **4a** in water was found to be less favorable by 7.9 kcal mol^{-1} than that in the gas phase. It has to be emphasized that the overall reaction **2a** → **4a** was found to be exothermic in both the gas phase (−2.1 kcal mol^{-1}) and water (−5.5 kcal mol^{-1}). No siginificant acceleration by protic solvents was expected for the tautomerization of **2a** to **1a** because this reaction involves a carbon atom and proceeds as an H-atom transfer.[17] Specific effects of hydrogen bonding were not studied for this reaction, only bulk solvent effects were estimated by applying SCRF calculations to the TS and reactants (see Table 3). The effective barrier for the reaction *E*-**2a** → **1a** was predicted to increase by ∼5 kcal mol^{-1} in water as compared to the gas phase.

An activation barrier of 39.2 kcal mol^{-1} (B3LYP/6-311+G(2d,p)//B3LYP/6-31+G(d)) has been predicted for the isomerization of **2a**$^-$.[17] Again, hydrogen-bonded complexes with water were not explored for the anionic species and only bulk solvent effects on the isomerization were estimated by using the B3LYP/6-31+G(d) geometries optimized in the gas phase (see Table 2). The reaction **2a**$^-$ → **3a**$^-$ in water was predicted to be exothermic by 13 kcal mol^{-1}. A solvent-induced decrease by 7 kcal mol^{-1} was found for the activation energy of this process.

IRC Profiles for the Cyclization of the *aci* Form of 2-Nitrotoluene. The intrinsic reaction coordinate for the cyclization of *E*-**2a** and the analogous isomerization reaction of **2a**$^-$ was traced at the B3LYP level of theory with the 6-31G(d) and 6-31+G(d) basis sets, respectively. Figures 2 and 3 present the energy profiles together with variations in the selected internal coordinates along the IRC paths. The parameters of the minimum-energy structures are presented as horizontal bars placed at the ends of the IRC paths because the exact positions of the minima on the reaction coordinates are unknown. The minimum-energy structures were not reached in these calculations because of convergence problems. However, the remainder of the IRC paths accounted for <10% of the total energy change, and the bond lengths and angles at the final points of the IRC paths were almost identical to those of the equilibrium structures.

The IRC paths were analyzed starting from the *aci* form. Both *E*-**2a** and its anion **2a**$^-$ were predicted to be completely planar. The isomerization reaction was initiated by an out-of-plane distortion of the quinonoid intermediates that corresponded to sp^2-sp^3 hybridization changes in C_7 and N. This distortion was accompanied by gradual changes in the bond angles within the groups involving these two atoms. The disrotatory movement of the CH_2 and NOOH groups and the disruption of the π framework with the alternating single and double C−C bonds took place simultaneously so that the corresponding dihedrals and bond lengths reached intermediate values in the TS. In contrast, the bonds formed by the nitrogen atom were predicted to change nonsynchronously along the IRC. The bond lengths showed little change at initial steps of the reactions. The $N-O_{12}$ bond in **2a** remained practically constant when the IRC value changed from −6 to −2 amu$^{1/2}$ bohr and then lengthened by ∼2% in the TS. When the coordinate passed the transition point, this bond quickly elongated to reach a value increased by 14.8%

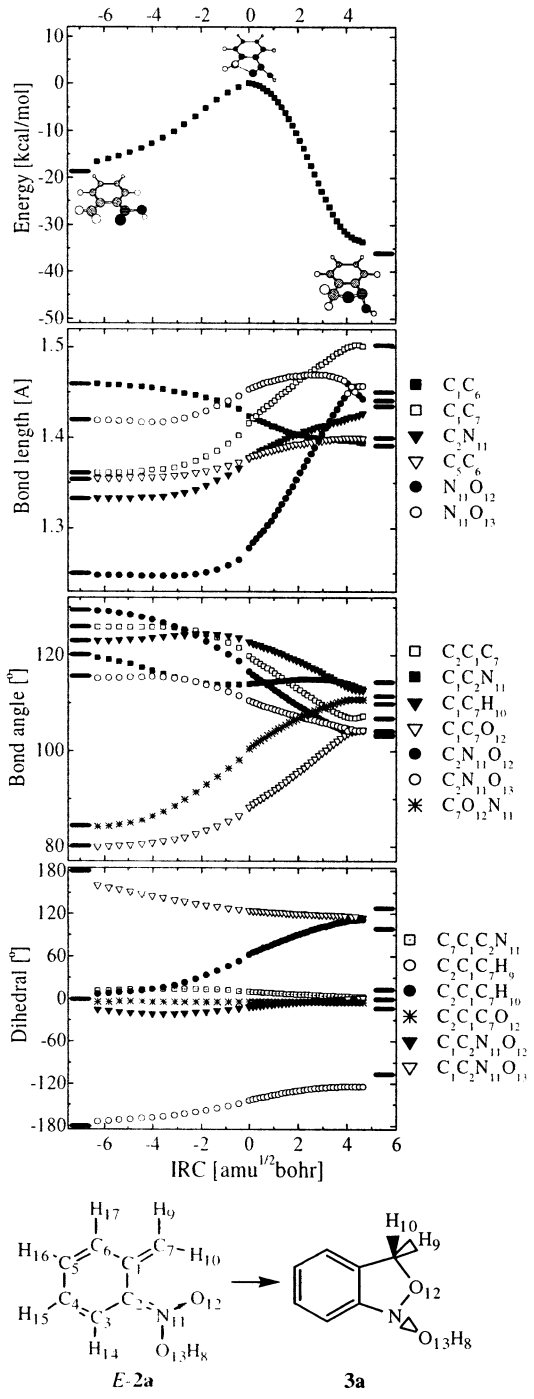

Figure 2. IRC profiles calculated at the B3LYP/6-31G(d) level for the isomerization of *E*-**2a**. The reaction scheme and atom numbering are also given.

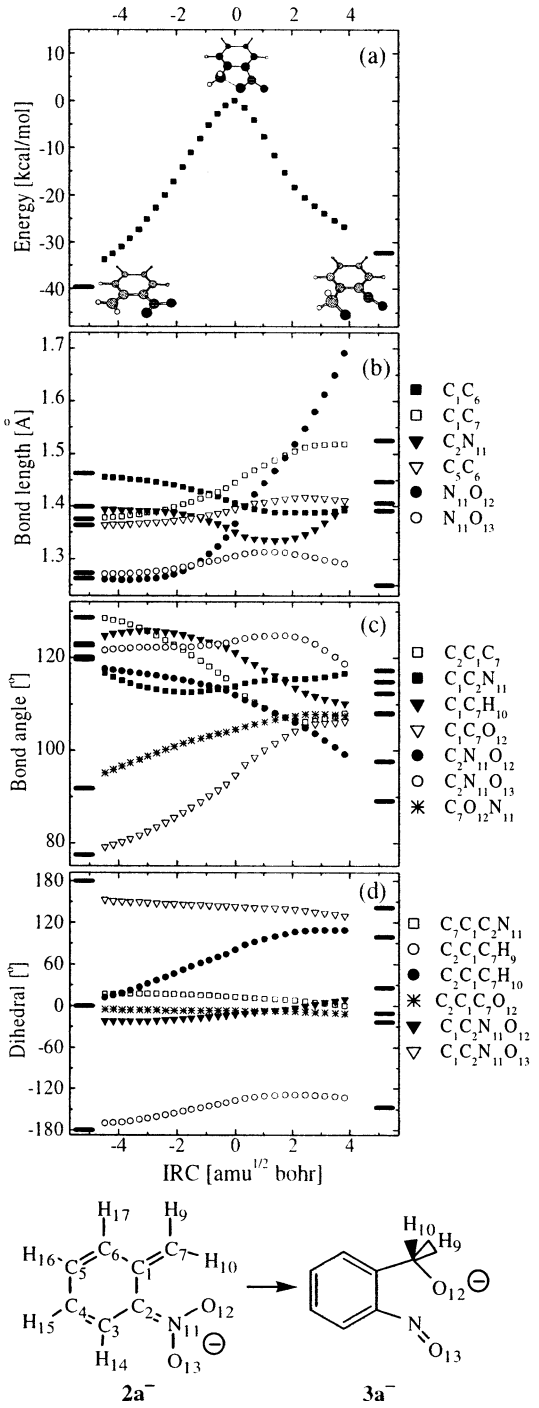

Figure 3. IRC profiles calculated at the B3LYP/6-31+G(d) level for the isomerization of **2a**$^-$. The reaction scheme and atom numbering are also given.

in **3a**. Variation of the N−O_{13} bond along the IRC showed a peculiar profile with a maximum. The maximum length of this bond exceeded that of *E*-**2a** and **3a** by 3.5 and 1.3%, respectively. Structural perturbations of **2a**$^-$ were predicted to be generally similar to those in *E*-**2a**, but some important differences were found. The C_2−N bond in the protonated form showed monotonic stretching along the reaction coordinate. In contrast, this bond in the anionic species first shortened by 3.4% in the TS and then elongated by approximately the same amount in the product **3a**$^-$. The N−O_{12} bond in **TS [2a**$^-$**−3a**$^-$**]** was elongated by 8.2%. This stretch eventually led to the breaking of the σ bond between the N and O_{12} atoms in **3a**$^-$. Quite different behavior of the C_2NO_{13} bond angle in the protonated form and the anion was also predicted. This angle in the nitronic acid first remained constant and then showed a monotonic decrease once the IRC passed −4 amu$^{1/2}$ bohr. In the anionic form, the C_2NO_{13} angle increased slowly and reached a maximum shortly after passing the TS. This angle was predicted to be smaller by 4.4% in **3a**$^-$ than in **2a**$^-$.

Cyclization and Tautomerization of the Quinonoid Intermediates. In the presence of an α substituent, four stereoisomers of the quinonoid intermediate **2** may be formed and each of these isomers may exist in several conformations. Our results[17] for the parent compound suggested significantly lower barriers for the cyclization of the *E* isomers of **2**. Here, *E* and *Z* indicate the relative position of the *N*-hydroxyl group. Moreover, the *E*

isomers are expected to be more stable and therefore dominate in a reaction mixture. Even if these isomers would not be populated directly via the triplet-state tautomerization of **1**, they would be rapidly formed in solution through proton transfer reactions. Therefore, the cyclization of only two isomers (*EE* and *EZ* in Scheme 2) was explored in detail. It should be noted that the stereoisomers are labeled in such a way as to facilitate comparison among different compounds. These designations may differ from abbreviations that may be constructed from the chemical names corresponding to the IUPAC recommendations.

2,1-Benzisoxazolines may exist in two isomeric forms, *E*-**3** and *Z*-**3**, which differ in the relative position of the X and OH group. These two isomers may also adopt different conformations. The activation barrier for the isomerization *Z*-**3** → *E*-**3** via nitrogen inversion is expected to be high because of the presence of two oxygen atoms.[37] From the B3LYP/6-311+G(2d,p) energies computed at the B3LYP/6-31G(d) geometries, we obtained estimates of 16.8, 16.7, and 18.0 kcal mol^{-1} for this barrier in *Z*-**3** derived from **2a**,[17] **2i**,[19] and 2-nitrobenzyl methyl ether (**2j**),[18] respectively. To locate the TS connecting **2** and **3**, all possible combinations of the isomers of **2** and **3** taken in their lowest-energy conformations were used. The cyclization of *EE*-**2** resulted exclusively in the *Z* isomer of **3**. The *EZ* isomer of **2** afforded *E*-**3** for all derivatives studied. Our extensive efforts to locate other TSs failed. Typical molecular structures are depicted in Figure 4a.

In addition, TSs corresponding to an H-atom shift between the O_{12} and C_7 atom in the *ZZ* and *ZE* isomers of **2** were located. The B3LYP/6-31G(d) optimized geometries of the TSs and the corresponding conformers of nitro compounds **1c** and **1j** are depicted in Figure 5. Numerous attempts to locate a TS for the 1,5-hydrogen shift in different conformers of **1h** (X = NH_3^+) failed.

Full geometry optimization at the B3LYP/6-31+G(d) level was also performed for anionic species produced by deprotonation of **1**−**4**. The B3LYP/6-31G(d) geometry of a protonated species without the proton H_8 (see Scheme 2) was used as an initial guess for an anion. Nitro compounds (**1**) and nitronic acids (**2**) were demonstrated to share common anions (**2**$^-$). For all α substituents studied, geometry optimization of the deprotonated bicyclic intermediates (**3**) yielded anions (**3**$^-$) which showed surprisingly little similarity with the parent compounds. Rather, these anions may be classified as particular conformers of 2-nitroso compounds (**4**) in the deprotonated form. The commonness of the anionic species for **3** and **4** was confirmed for the isomers of **1j**. The same minimum was reached in the geometry optimization for anions produced from the following couples of the acids: *anti*-**1j** and *EE*-**2j** (*E*-**2j**$^-$); *syn*-**1j** and *EZ*-**2j** (*Z*-**2j**$^-$); *E*-**3j** and *syn*-**4j** (*E*-**3j**$^-$); *Z*-**3j** and *anti*-**4j** (*Z*-**3j**$^-$). The molecular structures of several anions are shown in Figure 4b. For clarity's sake and by analogy, the two anions obtained from *E*-**3** and *Z*-**3** were labeled as stereoisomers. However, they should be more properly referred to as *anti* and *syn* conformers. Stereoselectivity of the anion isomerization appeared to be similar to that for the protonated form: anionic TSs could be located only for the reactions *E*-**2**$^-$ → *Z*-**3**$^-$ and *Z*-**2**$^-$ → *E*-**3**$^-$.

Total and zero-point energies for all the stationary points found in this study are presented in Tables 1S and 2S in Supporting Information. The total energies were computed by using four different hybrid functionals in combination with the 6-311+G(2d,p) basis set. Solvation effects were estimated from the single-point free energies computed within the PCM model at the B3LYP/6-31G(d) geometries optimized in the gas-phase.

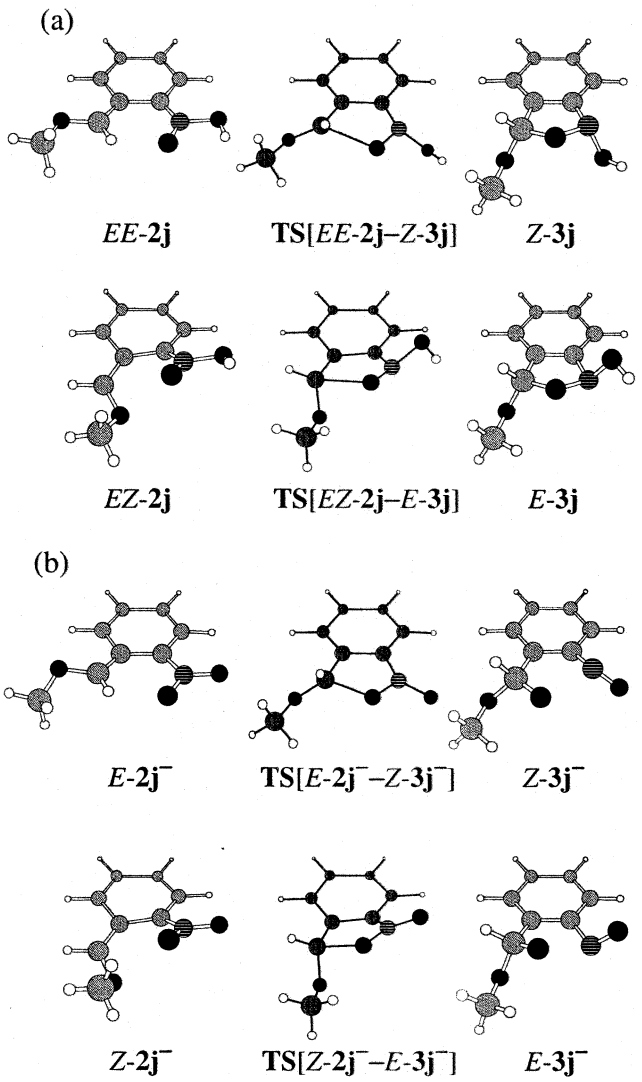

Figure 4. (a) The B3LYP/6-31G(d) optimized geometries of the two stereoisomers of **2j** and **3j**, along with the transition structures connecting them. (b) The B3LYP/6-31+G(d) optimized geometries of the two stereoisomers of **2j**$^-$ and two conformers of **3j**$^-$ along with the transition structures connecting them.

Activation energies were calculated as differences between the sZPE-corrected total energies or free energies of the TSs and the quinonoid intermediates **2**. Rather than using the energies of *ZZ*-**2** and *ZE*-**2**, apparent activation energies for the overall reaction **2** → **1** were obtained from the energies of the two more stable isomers (*EE*-**2** and *EZ*-**2**), which were shown to undergo the cyclization reaction. The results for **2** and **2**$^-$ with the different α substituents are summarized in Tables 1−3. For *EZ*-**2i**, a particular conformer with an intramolecular hydrogen bond was selected for presentation. The cyclization of another conformer (not shown) without hydrogen-bonding interactions between the OH and NOOH group was also explored. At the B3LYP/6-311+G(2d,p) level, its reaction was predicted to be exothermic by 20.1 kcal mol^{-1} and has an activation energy of 13.8 kcal mol^{-1}. These parameters were close to those obtained for the cyclization of the methyl ether, *EZ*-**2j**. Table 3 also presents estimates for the relative yield (η) of formation of **3**. These quantities were calculated from the ratio of the exponential factors with the activation energies for the cyclization and retautomerization of **2**. Under the assumption that both reactions are characterized by a single rate constant with the same preexponential factor and the formation of **3** is irreversible,

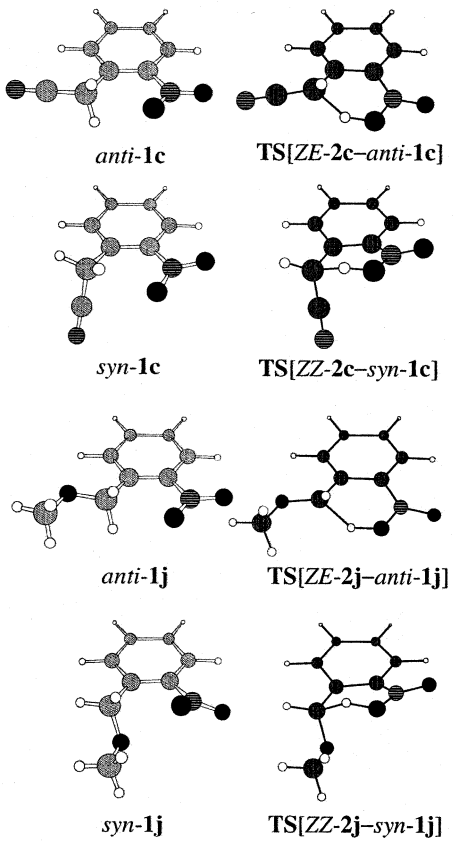

Figure 5. B3LYP/6-31G(d) optimized geometries of the two conformers of **1c** and **1j** along with the transition structures for their tautomerization.

η gives a good idea of the efficiency of the overall ground-state isomerization reaction.

Structure−Reactivity Relationships. Plots of the computed activation energies (E_a) vs reaction energies (ΔE) for the cyclization of **2** and for the corresponding reaction of $\mathbf{2}^-$ in the gas phase are presented in Figure 6a. Analogous data obtained from the total free energies in water are shown in Figure 6b. A linear fit to the entire set of the "cyclization" data (Figure 6a) yielded a slope of 0.866 and an intrinsic barrier of 30.6 kcal mol^{-1} (activation energy for the zero reaction energy) with a correlation coefficient $R = 0.849$. When only the data for the protonated form were fitted, a slope of 0.236 and a much smaller intrinsic barrier of 18.9 kcal mol^{-1} ($R = 0.382$) were obtained. One could hardly recognize any relationship between E_a and ΔE for the "cyclization" in water. The best linear fit for the entire set of data had a correlation coefficient of 0.433. Effective activation energies (E_a^{eff}) plotted against ΔE for the tautomerization **2** → **1** are shown in Figure 6, parts c and d. Linear regression analysis gave slopes of 0.664 ($R = 0.823$) and 0.508 ($R = 0.792$) for the data in the gas phase and water, respectively. Intrinsic barriers of 31.6 and 33.4 kcal mol^{-1} were obtained for this process in the gas phase and aqueous solution.

Figure 7 presents the calculated activation barriers for the cyclization and tautomerization of **2** that are plotted against the Hammett-type substituent constants, σ_p^+. These parameters, rather than the Hammett constants (σ_p), have been adopted as descriptors for the para substituents conjugated with the reaction center.[38] When compared to three alternative parameters (σ_m, σ_p, and σ_p^-), the σ_p^+ constants also appeared to be slightly better descriptors for the reactions of **2**. The σ_p^+ values for the substituents in **2g**, **2h**, and **2k** could not be found in the literature and were approximated by using the reported values[38b] for NHCOMe, NMe_3^+, and OCOMe, respectively. The best fits shown in Figure 7 had correlation coefficients of 0.903 and 0.844 for the cyclization data in the gas phase and water, respectively. The effective activation energies of the tautomerization in the gas phase and water were fitted with correlation coefficients of −0.881 and −0.859. The fitting parameters are shown in Figure 7. The data for *EZ*-**2f**, *EZ*-**2h**, and a particular conformer of *EZ*-**2i** were not included in this analysis. Strong intramolecular hydrogen bonds formed by the α substituent and the O_{12} atom were responsible for surprisingly high activation barriers in these molecules. The points corresponding to *EE*-**2f**, *EE*-**2i**, and a conformer of *EZ*-**2i** without the intramolecular H bond definitely fall within the scatter range (see Figure 7).

TABLE 1: Energies of the Bicyclic Intermediates (3) and the Transition Structures for the Reaction 2 → 3 Calculated in kcal mol^{-1} Relative to the Energy of *EE*-2 or *EZ*-2

		gas phase				water
substituent	molecule	*a*	*b*	*c*	*d*	*e*
		EE-**2** → *Z*-**3**				
H	**3a**	−14.2	−22.7	−15.3	−16.1	−22
H	**TS [*E*-2a−3a]**	18.2	22.4	19.0	18.2	20
CH_3	*Z*-**3b**	−16.2	−25.4	−17.6	−17.8	−22
CH_3	**TS [*EE*-2b−*Z*-3b]**	14.9	18.4	15.4	14.8	14
CN	*Z*-**3c**	−4.7	−14.9	−6.4	−6.2	−15
CN	**TS [*EE*-2c−*Z*-3c]**	19.1	23.3	19.7	18.9	17
F	*Z*-**3d**	−19.5	−28.6	−21.1	−21.3	−27
F	**TS [*EE*-2d−*Z*-3d]**	14.2	17.6	14.6	14.0	11
Cl	*Z*-**3e**	−17.2	−25.7	−18.7	−18.5	−27
Cl	**TS [*EE*-2e−*Z*-3e]**	14.9	18.7	15.3	14.7	14
NH_2	*Z*-**3f**	−11.4	−20.6	−13.0	−13.0	−15
NH_2	**TS [*EE*-2f−*Z*-3f]**	9.7	11.8	10.0	9.8	7
NHCHO	*Z*-**3g**	−11.8	−21.4	−13.4	−13.5	−20
NHCHO	**TS [*EE*-2g−*Z*-3g]**	12.1	14.8	12.5	12.1	11
NH_3^+	*Z*-**3h**	−21.7	−30.8	−23.1	−22.8	−26
NH_3^+	**TS [*EE*-2h−*Z*-3h]**	16.6	20.5	17.2	16.3	16
OH	*Z*-**3i**	−13.9	−23.0	−15.4	−15.6	−22
OH	**TS [*EE*-2i−*Z*-3i]**	13.0	15.9	13.4	12.8	9
OCH_3	*Z*-**3j**	−13.4	−22.7	−14.9	−15.1	−24
OCH_3	**TS [*EE*-2j−*Z*-3j]**	12.3	15.2	12.7	12.4	8
OCHO	*Z*-**3k**	−15.0	−25.4	−24.1	−16.5	−17
OCHO	**TS [*EE*-2k−*Z*-3k]**	14.5	12.2	17.7	15.0	14
		EZ-**2** → *E*-**3**				
CH_3	*E*-**3b**	−20.7	−29.9	−21.9	−21.9	−26
CH_3	**TS [*EZ*-2b−*E*-3b]**	14.7	18.0	15.2	14.8	13
CN	*E*-**3c**	−11.5	−22.7	−13.4	−12.9	−19
CN	**TS [*EZ*-2c−*E*-3c]**	16.1	19.7	16.6	16.1	14
F	*E*-**3d**	−26.5	−36.4	−28.1	−26.5	−35
F	**TS [*EZ*-2d−*E*-3d]**	14.6	17.7	15.1	14.6	11
Cl	*E*-**3e**	−23.4	−32.5	−24.9	−24.4	−33
Cl	**TS [*EZ*-2e−*E*-3e]**	15.6	19.6	16.2	15.7	13
NH_2	*E*-**3f**	−8.8	−17.9	−10.4	−10.0	−19
NH_2	**TS [*EZ*-2f−*E*-3f]**	18.7	21.3	19.0	19.2	16
NH_3^+	*E*-**3h**	−12.7	−19.2	−13.9	−13.5	−26
NH_3^+	**TS [*EZ*-2h−*E*-3h]**	20.8	25.5	21.4	20.6	19
OH	*E*-**3i**	−7.9	−16.4	−9.5	−9.0	−20
OH	**TS [*EZ*-2i−*E*-3i]**	21.7	24.6	21.5	22.0	18
OCH_3	*E*-**3j**	−20.3	−30.1	−21.4	−21.3	−31
OCH_3	**TS [*EZ*-2j−*E*-3j]**	11.8	14.7	12.6	12.5	10

[a] B3LYP/6-311+G(2d,p)+sZPE//B3LYP/6-31G(d). [b] BHLYP/6-311+G(2d,p)+sZPE //B3LYP/6-31G(d). [c] B1LYP/6-311+G(2d,p)+sZPE //B3LYP/6-31G(d). [d] B3PW91/6-311+G(2d,p)+sZPE //B3LYP/6-31G(d). [e] SCRF−PCM, B3LYP/6-311+G(2d,p)//B3LYP/6-31G(d), total free energies were used.

Molecular Geometries of 1−3 and Transition Structures Connecting Them. Cartesian coordinates for all stationary points are available as Supporting Information, the atom numbering shown in Scheme 2 and Figures 2 and 3.

The B3LYP calculations predicted that the C_7 and N_{11} atoms hardly deviate from the plane of the benzene ring in both

TABLE 2: Energies of the Anions 3^- and the Transition Structures for the Reaction $2^- \rightarrow 3^-$ Calculated in kcal mol^{-1} Relative to the Energy of *E*-2^- or *Z*-2^-

		gas phase				water
substituent	molecule	*a*	*b*	*c*	*d*	*e*
	E-**2**$^-$ → *Z*-**3**$^-$					
H	**3a**$^-$	7.9	7.5	7.6	9.0	−13
H	**TS [2a**$^-$**−3a**$^-$**]**	39.3	43.5	40.0	39.0	32
CH_3	*Z*-**3b**$^-$	3.3	2.3	2.9	4.9	−16
CH_3	**TS [***E*-**2b**$^-$**−***Z*-**3b**$^-$**]**	34.9	38.8	35.6	34.8	27
CN	*Z*-**3c**$^-$	18.2	15.1	17.3	20.3	1
CN	**TS [***E*-**2c**$^-$**−***Z*-**3c**$^-$**]**	46.9	50.9	47.5	47.2	28
F	*Z*-**3d**$^-$	−14.5	−16.3	−15.2	−12.0	−35
F	**TS [***E*-**2d**$^-$**−***Z*-**3d**$^-$**]**	29.1	34.5	30.0	28.7	24
NH_2	*Z*-**3f**$^-$	−3.3	−5.3	−4.0	−1.6	−14
NH_2	**TS [***E*-**2f**$^-$**−***Z*-**3f**$^-$**]**	26.5	29.5	27.1	26.3	21
OH	*Z*-**3i**$^-$	−9.3	−11.9	−10.1	−7.5	−20
OH	**TS [***E*-**2i**$^-$**−***Z*-**3i**$^-$**]**	29.1	33.1	29.8	28.8	23
OCH_3	*Z*-**3j**$^-$	−6.8	−9.3	−7.5	−5.0	−26
OCH_3	**TS [***E*-**2j**$^-$**−***Z*-**3j**$^-$**]**	29.8	33.6	30.5	29.4	21
	Z-**2**$^-$ → *E*-**3**$^-$					
CN	*E*-**3c**$^-$	9.0	5.8	8.1	11.1	−5
CN	**TS [***Z*-**2c**$^-$**−***E*-**3c**$^-$**]**	37.7	43.4	38.5	38.1	29
NH_2	*E*-**3f**$^-$	0.8	−0.03	0.5	1.9	−12
NH_2	**TS [***Z*-**2f**$^-$**−***E*-**3f**$^-$**]**	32.5	35.0	32.9	32.3	28
OH	*E*-**3i**$^-$	0.08	−4.1	−1.1	2.7	−15
OH	**TS [***Z*-**2i**$^-$**−***E*-**3i**$^-$**]**	37.9	40.2	38.2	37.7	28
OCH_3	*E*-**3j**$^-$	−13.9	−16.4	−14.6	−12.0	−32
OCH_3	**TS [***Z*-**2j**$^-$**−***E*-**3j**$^-$**]**	25.7	29.6	26.5	25.4	22

[a] B3LYP/6-311+G(2d,p)+sZPE//B3LYP/6-31+G(d). [b] BHLYP/6-311+G(2d,p)+sZPE//B3LYP/6-31+G(d). [c] B1LYP/6-311+G(2d,p)+sZPE//B3LYP/6-31+G(d). [d] B3PW91/6-311+G(2d,p)+sZPE //B3LYP/6-31+G(d). [e] SCRF−PCM, B3LYP/6-311+G(2d,p)//B3LYP/6-31+G(d), total free energies were used.

conformers of **1**. According to experimental[39] and computational data,[17,39] the NO_2 group in **1a** is twisted relative to this plane. The twisting angle in the substituted compounds was found to vary substantially. The largest angle of 32° was obtained for *syn*-**1j**. In contrast, the NO_2 group in the *anti* conformers of **1d**, **1h**, **1i**, and **1j** was situated practically in the ring plane. The O_{12} and H_8 atoms in *syn*-**1b**, **1c**, **1f**, and **1i** were shifted from the benzene ring plane in the opposite directions (similar configurations were predicted for the majority of *anti* conformers). A single minimum-energy structure that could be located for the *syn* conformers of all other derivatives has these atoms placed on the same side of the ring. Except for the C_1-C_7 bond, the lengths of all comparable bonds were predicted to be practically identical in substituted *anti*-**1** and *syn*-**1**. The C_1-C_7 bond was only slightly stretched in the substituted nitro compounds, the largest deviation of 1.8% (here and below, relative to the corresponding parameter of **1a**) was found for the amine *anti*-**1f**. The nonbonded distance H_8-O_{12} was predicted to be 2−10% shorter in the substituted compounds. The shortest distances of 2.228 and 2.337 Å were obtained for *syn*-**1e** and *anti*-**1h**. This shortening in *anti*-**1** resulted almost exclusively from narrowing the $C_2C_1C_7$ angle.

The TSs for the 1,5 hydrogen shift in **1a**−**1k** were found to be the "late" ones, resembling the products (*ZZ*-**2** and *ZE*-**2**) with alternating single and double C−C bonds. The $O_{12}-H_8$ bond was formed to a large extent, and the C_7-H_8 bond was practically broken in these TSs. The $O_{12}-H_8$ distances were significantly larger in the two TSs corresponding to **1f** (1.155 and 1.178 Å) than those in the TSs for **1c** (1.090 and 1.110 Å). Values in the range 134−148° were predicted for the $C_7H_8O_{12}$ angle in the tautomerization TSs.

The quinonoid moiety of *EE*-**2** derivatives was found to be essentially planar for all compounds except **2g** and **2k**, which showed deviations of 5−6° for the descriptive dihedrals. The largest differences in the bond length (∼2%, here and below relative to the corresponding parameter of *E*-**2a**) were found for the C_1-C_7 bond and both N−O bonds. The nonbonded distance between C_7 and O_{12} was generally shorter in the substituted nitronic acids. The largest deviation of 4.2% was found for **2h**. The interplay between bond length variations (C_1-C_7 and $N_{11}-O$) and slight narrowing of the $C_2C_1C_7$ angle caused this shortening.

Molecular structures of *EZ*-**2a**−*EZ*-**2k** strongly deviated from planarity. Repulsive interactions between the α substituent and the nitronic moiety led not only to displacement of the atoms located outside the six-membered ring but also to a distortion of the ring. The $C_6C_1C_2C_3$, $C_6C_1C_2N_{11}$, and $C_7C_1C_2C_3$ torsion angles varied in the range 12−28°. *EZ*-**2b** showed the largest distortions. Substituent effects on the bond lengths in the *EZ*-**2** derivatives were comparable to those in the *EE*-isomers. Extra lengthening of the $N-O_{12}$ bond due to hydrogen bonding was demonstrated by comparing structural parameters of two conformers of *EZ*-**2i**. The $N_{11}-O_{12}$ bond was stretched by 3.8%

TABLE 3: Energies of 2-Nitrobenzyl Derivatives (1) and the Transition Structures for the Reaction 2 → 1 Calculated in kcal mol^{-1} Relative to the Energy of *EE*-2 or *EZ*-2

		gas phase/*a*		gas phase/*b*		water/*c*	
substituent	molecule	energy	η^d	energy	η^d	energy	η^d
	EE-**2** → → *anti*-**1**						
H	**1a**	−27.6		−30.5		−27	
H	**TS [***Z*-**2a−1a]**	13.7	0.1	18.1	0.2	19	0.4
CH_3	*anti*-**1b**	−23.7		−27.1		−24	
CH_3	**TS [***ZE*-**2b−***anti*-**1b]**	15.0	0.5	19.5	0.6	20	0.9
CN	*anti*-**1c**	−19.4		−24.3		−20	
CN	**TS [***ZE*-**2c−***anti*-**1c]**	13.7	0.1	16.5	0.1	19	0.7
F	*anti*-**1d**	−24.2		−28.0		−24	
F	**TS [***ZE*-**2d−***anti*-**1d]**	17.5	0.8	22.6	0.9	23	1.0
Cl	*anti*-**1e**	−23.2		−27.0		−23	
Cl	**TS [***ZE*-**2e−***anti*-**1e]**	15.6	0.6	19.9	0.6	22	1.0
NH_2	*anti*-**1f**	−12.6		−16.1		−10	
NH_2	**TS [***ZE*-**2f−***anti*-**1f]**	24.1	1.0	30.4	1.0	29	1.0
NHCHO	*anti*-**1g**	−17.0		−20.7		−20	
NHCHO	**TS [***ZE*-**2g−***anti*-**1g]**	20.3	1.0	25.9	1.0	23	1.0
NH_3^+	*anti*-**1h**	−19.1		−22.9		−29	
OH	*anti*-**1i**	−18.3		−21.9		−18	
OH	**TS [***ZE*-**2i−***anti*-**1i]**	20.4	1.0	26.1	1.0	24	1.0
OCH_3	*anti*-**1j**	−18.8		−22.7		−19	
OCH_3	**TS [***ZE*-**2j−***anti*-**1j]**	20.4	1.0	26.0	1.0	25	1.0
OCHO	*anti*-**1k**	−20.8		−24.4		−23	
OCHO	**TS [***ZE*-**2k−***anti*-**1k]**	18.8	0.9	23.1	0.9	24	1.0
	EZ-**2** → → *syn*-**1**						
CH_3	*syn*-**1b**	−28.4		−32.1		−27	
CH_3	**TS [***ZZ*-**2b−***syn*-**1b]**	14.2	0.4	18.7	0.6	19	0.9
CN	*syn*-**1c**	−24.5		−30.2		−26	
CN	**TS [***ZZ*-**2c−***syn*-**1c]**	10.8	0.1	12.7	0.1	16	0.7
F	*syn*-**1d**	−28.6		−33.0		−31	
F	**TS [***ZZ*-**2d−***syn*-**1d]**	17.2	0.8	22.1	0.9	23	1.0
Cl	*syn*-**1e**	−30.4		−34.9		−31	
Cl	**TS [***ZZ*-**2e−***syn*-**1e]**	13.1	0.3	16.9	0.3	18	0.9
NH_2	*syn*-**1f**	−11.2		−14.6		−12	
NH_2	**TS [***ZZ*-**2f−***syn*-**1f]**	29.5	1.0	36.8	1.0	33	1.0
NH_3^+	*syn*-**1h**	−22.8		−25.5		−29	
OH	*syn*-**1i**	−12.6		−15.1		−16	
OH	**TS [***ZZ*-**2i−***syn*-**1i]**	32.8	1.0	40.5	1.0	36	1.0
OCH_3	*syn*-**1j**	−24.1		−28.3		−26	
OCH_3	**TS [***ZZ*-**2j−***syn*-**1j]**	18.9	1.0	24.7	1.0	24	1.0

[a] B3LYP/6-311+G(2d,p)+sZPE//B3LYP/6-31G(d). [b] BHLYP/6-311+G(2d,p)+sZPE //B3LYP/6-31G(d). [c] SCRF−PCM, B3LYP/6-311+G(2d,p)// B3LYP/6-31G(d), total free energies were used. [d] Relative efficiency of the formation of **3** calculated as $\eta = (1 + \exp[-(E_a^t - E_a^c)/RT])^{-1}$, where E_a^t and E_a^c are the effective activation energies for the tautomerization and cyclization.

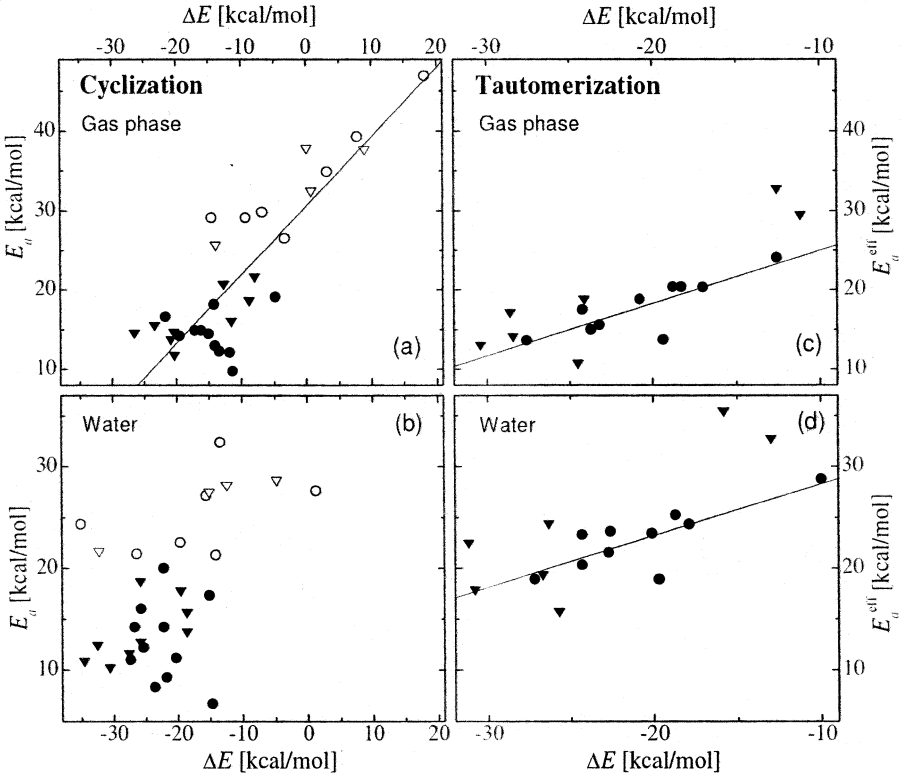

Figure 6. Computed activation energies plotted against reaction energies for the cyclization (a, b) and tautomerization (c, d) of *EE*-**2** (solid circles) and *EZ*-**2** (solid triangles) in the gas phase (a, c) and in water (b, d). Analogous data for the isomerization of the deprotonated species (open symbols) are also shown. The B3LYP/6-311+G(2d,p) single-point energies corrected for sZPE and total free energies were used for the gas phase and water, respectively; the energies were computed at the B3LYP geometries optimized in the gas phase with the 6-31G(d) and 6-31+G(d) basis set for the nitronic acids and their anions, respectively; solvation effects were estimated with the SCRF-PCM method.

in a conformer with an intramolecular hydrogen bond ($O_9H\cdots O_{12}$) and only by 1.0% in that without such a bond. The C_7-O_{12} distance increased significantly in the *Z* isomers. The largest value of 3.009 Å (8.1% increase) was predicted for this distance in *EZ*-**2b**.

Substituent effects on the molecular structure of **3** were more pronounced than those for **1** and **2**. All bicyclic compounds studied adopted an envelope-like conformation with the O_{12} atom out of the plane of the rest of the molecule. The *Z* isomers were found to exist in a *trans*-envelope conformation with the $O_{13}H_8$ group in a pseudoaxial position ($C_1C_2N_{11}O_{13} \sim 100-130°$). The conformational choice of the five-membered ring in the *E* isomers appeared to be very sensitive to the α substituent. Numerous optimization runs with different starting geometries yielded a single conformational minimum for all compounds *E*-**3** except *E*-**3i**. The latter molecule showed two conformations depending on the orientation of the OH on the C_7 atom. A pseudoaxial conformation was found for the *E* isomers of **3b**, **3c**, and **3f**. The hydroxy group in the pseudoequatorial position was predicted for **3d**, **3e**, **3h**, and **3j**. The configuration of the N_{11} atom in **3** was also affected by the α substituent. The largest variations in the dihedrals including the N_{11} atom were found for the amine **3f** and its protonated form **3h**.

Despite pronounced differences in the minimum-energy conformations of *E*- and *Z*-**3**, variations in the bond lengths and angles with the α substituent appeared to be rather similar for both isomers. These variations were localized on the five-membered ring. The C_7-O_{12} bond appeared to be the most susceptible to the presence of the substituent. It was shorten by 4.0 and 6.0% in *Z*-**3h** and *E*-**3h**, respectively, and elongated by ~2.0% in both isomers of **3f** (here and below, relative to the corresponding parameter of **3a**). The bond lengths in the other compounds were within the range provided by **3f** and **3h**. Generally, the $N-O_{12}$ bond was stretched and the $N-O_{13}$ bond was shorten in the substituted **3**. The five-membered ring in the *E* isomers with the pseudoequatorial position of the OH group was highly asymmetric with the O_{12} atom shifted toward the C_7 atom. The largest distortions by +7.7% and −5.2% were predicted for the $N-O_{12}$ and $N-O_{13}$ bond lengths in *E*-**3h**.

The bond angles affected by the substituent X were centered at the C_7 and N_{11} atoms. Generally, the protonated amine **3h** provided the largest deviations for the bond angles. The $N_9C_7O_{12}$ angle in *Z*-**3h** and *E*-**3h** was reduced by 5.1 and 8.2%, respectively. The two other angles formed by the C_7 and N_9 atoms, $C_2N_{11}O_{12}$ and $ON_{11}O$, were also considerably smaller in the **3h** isomers. Contrary, the $C_1C_7H_{10}$, $C_1C_7O_{12}$, and $H_{10}C_7O_{12}$ angles were widened by 3−5% in the *E*- and *Z*-**3h**. Structural distortions in **3h** could not be assigned exclusively to hydrogen-bonding interactions or electronic effects because similar distortions were found in halogen-substituted compounds (**3d** and **3e**) but not in the nitrile (**3c**).

TSs for the cyclization of *EE*-**2** and *EZ*-**2** were predicted to be nonplanar. The configuration of the $C_7X_9H_{10}$ and NOOH groups could be characterized as intermediate between those predicted for the reactant and product. The largest variation (±6%) in the bond lengths was found for the C_7-O_{12} distance, which was generally smaller in substituted compounds. The C−C bond lengths for the six-membered ring of the TS reached values that were close to mean values for the corresponding distances in **2** and **3**. In contrast, the $N-O_{12}$ bond in the TSs was only slightly elongated so that its length remained much smaller than that in **3**.

Molecular Geometries of the Deprotonated Form of 1−3 and Transition Structures Connecting Them. Deprotonation of all the molecules **1**−**3** was accompanied by substantial

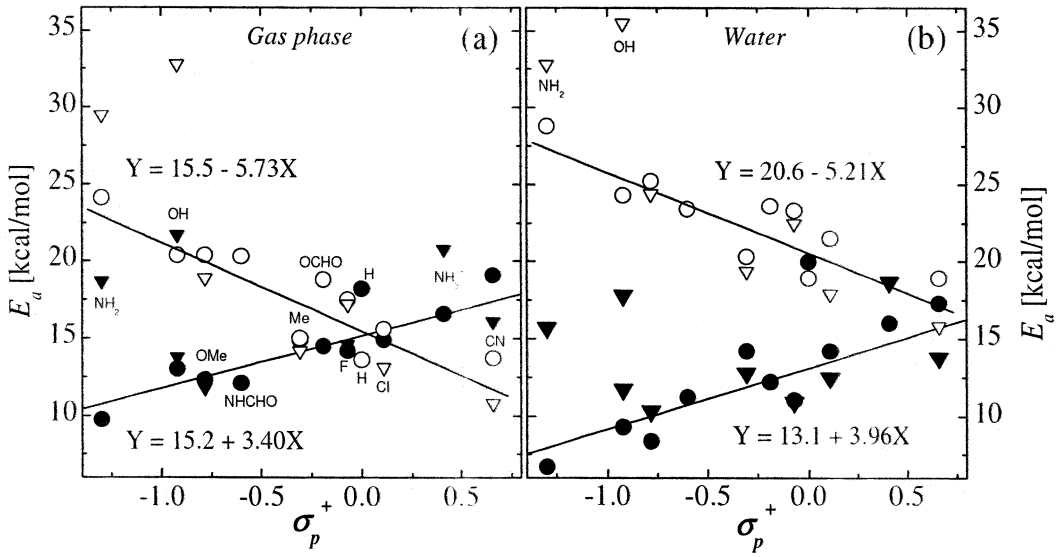

Figure 7. Plots of activation energies vs the Hammett-type σ_p^+ constants of the α substituents. The activation barriers for the cyclization **2** → **3** (solid symbols) and tautomerization **2** → **1** (open symbols) were computed in the gas phase (a) and water (b). Explanations for the energy calculations are given in Figure 6. The σ_p^+ constants are taken from ref 38b. The linear equations correspond to the best fits to the data (shown as solid lines). Circles represent the reactions of *EE*-**2**; triangles, *EZ*-**2**.

changes in the geometry, those for **3**$^-$ being the largest ones. The quinonoid moiety of *E*-**2**$^-$ was predicted to be planar for all compounds except **2f** and **2j**, which showed deviations in the dihedrals in the range 2−6°. Nonplanar structures and substantial variations in the torsion angles were found for the *Z* isomers of **2**$^-$. The bond lengths in substituted *E*- and *Z*-**2**$^-$ were predicted to be similar to those in **2a**$^-$, the largest deviation being 1.9% stretch of the C_1-C_7 bond in **2c**$^-$. Generally, the C_7-O_{12} distance was slightly shorter (1−4%) in the substituted anions *E*-**2**$^-$. This distance was reduced by 10.1% in *Z*-**2c**$^-$ and increased by 6.5% in *Z*-**2f** $^-$. The $N_{11}-O_{12}$ bond was elongated and C_2-N_{11} shortened in *Z*-**2f**$^-$ and *Z*-**2i**$^-$ due to strong H-bonding interaction between the substituents and the O_{12} atom.

Although pronounced variations in the geometry of the anions obtained upon deprotonation of **3** were found, several common features could be revealed. The $N_{11}-O_{12}$ distance of 2.1−2.5 Å indicated that this bond was practically broken in both isomers of **3**$^-$ for all substituents studied. Many structural parameters of **3**$^-$ resembled those of the deprotonated form of nitroso compounds (**4**). The $N_{11}-O_{12}$ distance was generally longer and the C_7-O_{12} bond was shorter in the substituted anions than that in **3a**. The C_7-O_{12} bond length in *Z*-**3d**$^-$ was reduced by 7.0%.

Very similar bond lengths were obtained for all the anionic TSs except those for the reactions *E*-**2c**$^-$ → *Z*-**3c**$^-$ and *Z*-**2c**$^-$ → *E*-**3c**$^-$. The C_1-C_7 and C_2-N_{11} bonds in the latter TSs were lengthened by 3−7%. In terms of the bond lengths, TSs for the **2**$^-$ isomerization can be characterized as "early" ones with the alternating C−C bond lengths in the six-membered ring and the elongated, but not broken, $N-O_{12}$ bond. Surprisingly large variations were found for the bond angles formed by the C_7 atom. These variations were largely responsible for different C_7-O_{12} distances in the anionic TSs.

Discussion

Interest in the reactivity of nitronic acids (**2**) is largely provoked by a role that these intermediates play in the photoisomerization of 2-nitrobenzyl compounds (**1**). Fast formation of **2** is the primary step in the photoinduced reaction of **1**. It is believed to occur in both the singlet and triplet excited state. Both excited states of the parent compound (**1a**) and several derivatives appeared to have sub-nanosecond lifetimes.[10,13,14,18,21,40] However, detailed information about excited-state dynamics is still not available. It is anticipated that quinonoid intermediates either result from a diabatic reaction of **1** or undergo very rapid nonradiative deactivation. Therefore, the ground-state reactivity of **2** is of primary importance for the overall isomerization process. Thermal reactions involving different stereoisomers of **2** may influence the efficiency and the rate of the release of the protected group, X. Dynamics and mechanism(s) of these reactions are still largely unknown. Recently, a detailed study of protolytic reactions of **1a** in aqueous solution was published.[20] Unfortunately, kinetic aspects of interconversions of the two stereoisomers of **2a** and of cyclization could not be unraveled. A very low quantum yield of **2a** indicated that tautomerization of **1a** could hardly account for very short lifetimes of the excited states. The major features of the ground-state potential energy surface of **1a** were determined in our computational studies. At the B3LYP/6-311+G(2d,p) level of theory, the lowest-energy path for the gas-phase isomerization of **1a** was characterized by an overall activation energy of 51.7 kcal mol^{-1}.[17] An activation barrier of 20.3 kcal mol^{-1} predicted for the reaction *Z*-**2a** → *E*-**2a** (see Scheme 1 and Figure 1) was substantially higher than an effective barrier of 9.7 kcal mol^{-1} for the retautomerization *Z*-**2a** ⟶ **1a**. A conformer of *Z*-**2a** directly involved in the 1,5 hydrogen shift was shown to undergo a practically barrierless rearrangement to a more stable conformer shown in Figure 1. In the gas phase, none of the reaction pathways leading to **4a** can compete with anthranil formation initiated by the $N-O_{13}$ bond fission in **3a**. It is noteworthy that the rate-determining step for the lowest-energy path leading to **4a** was identified as a 1,3-hydrogen shift in **3a** (see Figure 1).

In this work, computational methods were used to evaluate α-substituent effects on the rearrangements of nitronic acids and effects of protic solvents on these processes. The potential energy surface of **2a** in water was explored in detail. To account, at least partly, for specific interactions in the first solvation shell, hydrogen-bonded complexes with a single water molecule were optimized in the gas phase. Thereafter the polarizable continuum

model of Tomasi and co-workers[34] was employed to estimate bulk solvent effects. As expected, the activation barriers for solvent-assisted proton-transfer reactions decreased dramatically. A reduction by more than 10 kcal/mol was predicted for the activation barrier of the 1,3-hydrogen shift in **2a** and **3a**. These results are in reasonable agreement with previous findings for reactions of this type.[41] In contrast, the barrier height for the cyclization of *E*-**2a** was found to be practically the same in the gas phase and in water. Moreover, essentially the same barrier was predicted with SCRF-PCM calculations performed on the bare molecule *E*-**2a** and its complex with water. No drastic change in the barrier height for the retautomerization of **2a** into **1a** was expected. This was confirmed by an SCRF calculation for molecular species optimized in the gas phase (see Table 3). In water, a TS for the cyclization of *E*-**2a** was predicted to have the highest energy on the entire pathway leading to **4a**.

It is conceivable that the major computational results obtained for **2a** are applicable to substituted analogues. The data presented here and elsewhere[10] provided strong support for this view. One can therefore envision the following scenario for the photoinduced isomerization of 2-nitrobenzyl derivatives in protic solvents. The photoexcitation likely results in a mixture of four stereoisomers of **2**. However, equilibrium that is strongly shifted toward the more stable *E* isomers should rapidly (presumably on the nanosecond time scale) be established. The equilibration time may be even shorter in acidic solutions because of fast protolytic reactions. Temporal behavior of the protonated form of **2** is governed by the two competing processes: cyclization to **3** and retautomerization to **1**. The effective activation barriers for these two processes should basically determine the rate of the quinonoid intermediate decay that is usually reported in experimental studies. A difference between the effective activation energies for the two competing reactions of **2** may be used to estimate a contribution of the ground-state reactions to the overall quantum yield of the photoinduced isomerization of **1**. Therefore, characterization of the transition structures for the two rearrangements of **2** was of immediate interest. The rearrangement of the bicyclic intermediates **3** might also affect the quantum efficiency of the entire reaction. However, our results[17−19] obtained for **2a**, **2i**, and **2j** suggest that, generally, this is not the case because formation of **3** is practically irreversible. Nevertheless, the isomerization of **3** plays an important role in the photoinduced decomposition of **1** because it often determines the rate of the end product formation.

The cyclization of **2** leads to the formation of a new σ bond (C_7-O_{12}) and to profound changes in the configuration of the N_{11} and C_7 atoms. The reaction is accompanied by changes in the length of every bond in the reactant except the Y−H bonds. The results of the IRC calculations for **2a** underlined the complexity of the reaction **2** → **3**. Changes in the bond lengths did not develop synchronously when the molecule moved along the reaction coordinate. This was confirmed by analogous calculations for **2i** and **2j**.[18,19] Virtually no correlation between the barrier height and the C_7-O_{12} distance in the quinonoid intermediates was found. The DFT computations predicted exclusively a disrotatory closure for *EE*-**2** and a conrotatory one for *EZ*-**2**. Out-of-plane distortion of **2** appeared to correlate with the cyclization stereoselectivity but not with the reaction energetics. The reaction **2** → **3** was predicted to be highly favorable for all compounds studied. Except when an H bond between the substituent and O_{12} was formed, differences (<3 kcal mol^{-1}) between E_a for the cyclization of *EE* and *EZ* isomers were practically within the accuracy of the methods used. However, these differences are large enough to account for biexponential decay kinetics that has been observed for the *aci* form of several derivatives.[10,16,18,19] The B3LYP/6-311+G(2d,p) barrier height varied from 9.7 kcal mol^{-1} in *EE*-**2f** to 21.7 kcal mol^{-1} in *EZ*-**2i** with the intramolecular H bond. Generally, the barriers calculated with the B3LYP functional were underestimated by 3.3 ± 0.7 kcal mol^{-1} and the reaction energies were predicted to be less negative by 9.2 ± 0.9 kcal mol^{-1} when compared to the BHLYP results for the entire set of compounds. The results obtained with the B1LYP and B3PW91 functionals differed from those provided by the B3LYP method by less than 1.5 kcal mol^{-1}. Thus, they can be considered to be identical within the accuracy expected for these techniques. On the average, an increase by 8 ± 3 kcal mol^{-1} in the reaction exothermicity was predicted with the SCRF-PCM method for the cyclization of **2** in water. These data contrasted with a small average decrease (2 ± 1 kcal mol^{-1}) of the barrier height for this reaction in aqueous solution.

It is of interest to compare the cyclization of **2** with the 1,3-dipolar cycloaddition of nitrones. The latter process is one of the most extensively studied cycloaddition reactions.[42−44] Addition of the simplest nitrone to ethylene was a subject of numerous computational studies.[45,46] Generally, preference of a concerted single-step pathway was demonstrated and regioselectivity was correlated with the electron-donating ability of the dipolarphiles. The reaction of nitrones with monosubstituted olefins predominantly affords 5-substituted isoxazolidines, which are analogous to the five-membered ring in **3**. However, formation of 4-substituted derivatives was also observed in reactions of alkenes bearing strongly electron withdrawing substituents. This variation of the regioselectivity with the substituent compares well with the variation of the barrier height for the cyclization of **2**. In both cases, the process was strongly hindered by electron-withdrawing substituents.

The tautomerization **2** → **1** proceeds as a sigmatropic 1,5 hydrogen shift in a particular conformer of *ZE*- or *ZZ*-**2** with the OH group pointed toward the C_7 atom. These conformers are strongly destabilized by steric interactions and easily convert into more stable conformers such as *Z*-**2a** in Figure 1. The IRC calculations for **1a** and *anti*-**1i** confirmed the connectivity of the TSs to the corresponding conformers of the nitro compounds and their *aci* forms.[17,19] Because proton transfer equilibria are rapidly established in aqueous solutions, it is appropriate to use the total energies of more stable *E* isomers to estimate effective activation barriers (E_a^{eff}) for the reaction **2** → **1**. At the B3LYP level, the *E* isomers of **2a**−**2k** were destabilized by 13−30 kcal mol^{-1} relative to the nitro compounds, **1**. E_a^{eff} for retautomerization of *EE*- and *EZ*-**2** was predicted to vary in a slightly smaller range of 13−24 kcal mol^{-1} (see Table 3). The B1LYP and B3PW91 results were practically identical to those of the B3LYP technique. The BHLYP method generally overestimated the destabilization of **2** and the activation barriers. Averaged discrepancy between the BHLYP and B3LYP results was 3.8 ± 0.8 and 5.0 ± 1.5 kcal mol^{-1} for ΔE and E_a^{eff}, respectively. The SCRF-PCM calculations predicted only moderate solvation effects for the tautomerization process. On the average, practically no change in the reaction exothermicity and an increase by 5 ± 1 kcal mol^{-1} for the effective barrier height were found. One might expect that hydrogen bonding which was not accounted for in the PCM calculations would contribute to this increase of E_a^{eff} so that the retautomerization of **2** in aqueous solutions would be even more retarded.

The data presented in Figures 6 and 7 demonstrate that structural and environmental effects on the two isomerization reactions of **2** are quite different. When one considers the entire

set of data for the cyclization of **2** and the isomerization of $\mathbf{2}^-$ in the gas phase, one can see a tendency for a decrease in the barrier height with the reaction exothermicity. However, there exists no obvious interrelation between these two parameters for the reaction of the protonated species, **2**, in both water and gas phase. In contrast, E_a^{eff} for the tautomerization appeared to be well correlated with the reaction energy. This finding is in accord with the results for the molecular geometries of the transition structures. The TSs for the tautomerization can be characterized as "early" ones in relation to **2**. It is therefore not unexpected that the energy of these TSs is correlated with the energy gap between **1** and **2**. Contrary, the TSs for the cyclization possess rather peculiar geometries and can be considered as intermediate in several internal coordinates between **2** and **3**.

The results presented in Figure 6 suggest that computed energies of **2** and **3** can hardly be used to predict reactivity of the quinonoid intermediates toward the cyclization. Empirical correlations, such as the Hammett equation and its extended forms, are widely used in organic chemistry to analyze and interpret reaction mechanisms. Reasonably good correlations between the computed activation energies and the Hammett-type σ_p^+ constants for the substituent X were obtained in this study for both the cyclization and tautomerization. It is noteworthy that the energies of the frontier KS orbitals are also reasonably good descriptors of the reactivity of the neutral quinonoid intermediates toward cyclization (see Figure 1S in Supporting Information). These data suggest an approximately linear dependence of the KS eigenvalues for the occupied and unoccupied orbitals vs ionization potentials and electron affinities of **2** because the latter parameters are expected to be correlated with the σ_p^+ constants of the substituent. These findings are in agreement with recent observations that the orbitals in the original KS and hybrid schemes have more physical significance than originally anticipated.[47]

The activation barriers for the cyclization and tautomerization of **2** showed opposite trends with electron-donating ability of the substituent. The B3LYP data suggested that bicyclic intermediates (**3**) would be formed from **2** with a relative yield close to unity for all nitro derivatives except the parent compound and those with strong electron-withdrawing substituent(s) in nonpolar media. The same conclusion could be made when the BHLYP energies (see Tables 1 and 3) were used to estimate the yield. The fact that the overall photoisomerization yield varies substantially with substitution of **1** should be interpreted as evidence for strong variations in the quantum yield of the excited-state tautomerization. It is feasible that the barrier for the excited-state reaction is correlated with the relative stability of the product (**2**), which is predicted to increase with electron-donating ability of the α substituent. Thus, the results of this computational study suggest that both efficiency of the photodecomposition of **1** and the decay rate for **2** can be increased by introducing an electron-donating substituent in the α position. For bifunctional compounds, such as amino acids, an attachment to the nitrobenzyl moiety through the amino group should therefore be preferred. However, caution must be exercised if fast release of the protected group is of primary concern. Amino derivatives and other compounds with labile hydrogen(s) on the α substituent may afford a hydrated nitroso compound via an intramolecular proton transfer.[10,19] This mechanism should be the only one operating in the protonated amino derivatives, which are expected to have very high activation barriers for the cyclization (see data for **2h** in Table 1). The protected group release from the nitroso hydrates may be slower than that from **4**.

Deprotonation of **2** prevents its retautomerization to **1**, and hence, it might contribute to the increased isomerization efficiency. However, our computational data clearly demonstrated that aci anions ($\mathbf{2}^-$) were practically nonreactive species in relation to isomerization reactions. In this study, the SCRF-PCM method was used to estimate solvation effects on the isomerization of $\mathbf{2}^-$. Activation barriers predicted for the reaction $\mathbf{2}^- \rightarrow \mathbf{3}^-$ in aqueous solution (see Table 2) were higher than 20 kcal mol^{-1} for all derivatives studied and exceeded those for the cyclization of **2** at least by 10 kcal mol^{-1}. Thus, the decay of quinonoid intermediates in water should be completely controlled by reactions of the protonated form **2**, except extremely basic solutions where very slow reaction $\mathbf{2}^- \rightarrow \mathbf{3}^-$ might compete with the direct carbon protonation for some compounds. This finding is in excellent agreement with the experimental data for 2-nitrotoluene and some other derivatives.[18−20] Acidity of **2** is expected to decrease in the presence of an electron-donating substituent in the benzylic position. Thus, reactivity of such substituted compounds in aqueous solution at pH close to neutral should be enhanced not only due to generally lower activation barriers for reactions of protonated species but also due to a larger contribution of specific acid catalysis for compounds with higher pK_a.

Conclusions

Rearrangements of quinonoid intermediates (**2**) produced by the photoinduced isomerization of 2-nitrobenzyl derivatives were studied with DFT-based methods. An isomerization reaction of the *aci*-anions ($\mathbf{2}^-$) was predicted to encounter a much higher activation barrier than the cyclization of protonated species **2**. This suggests that specific acid catalysis should generally be observed for the decay of the *aci*-form of 2-nitrobenzyl derivatives. Pronounced effects of the α substituent on the activation barrier height for the cyclization and retautomerization of **2** were found. In contrast, only moderate solvation effects were predicted with the SCRF-PCM method for these processes in water. The results obtained with the B3LYP, B1LYP, and B3PW91 functionals may be considered as identical within the accuracy of the techniques used. Generally, the barriers calculated with the BHLYP functional were overestimated in comparison to the B3LYP results. However, both methods provided qualitatively consistent pictures for the reactivity of **2** and $\mathbf{2}^-$.

Two distinct reaction modes leading to two different stereoisomers of the bicyclic intermediate (**3**) were found for the cyclization of the two stereoisomers of **2**, differing in the position of the α substituent. Exclusively disrotatory closure was found for *EE*-**2** and only conrotatory mode of reaction was predicted for *EZ*-**2**. An important outcome from this study is the finding that both the relative stability of **2** and the activation barrier for the reaction $\mathbf{2} \rightarrow \mathbf{3}$ correlate with the electron-donating ability of the α substituent. The computational results suggested that performance of 2-nitrobenzyl compounds carrying a leaving group can be significantly improved by introducing an additional electron-donating substituent in the benzylic position.

Acknowledgment. The support of Kansas NSF Cooperative Agreement EPS-9874732 and the Wichita State University High Performance Computing Center is acknowledged. The author is greatly indebted to Prof. Jakob Wirz for generous support and stimulating discussions.

Supporting Information Available: Cartesian coordinates for **1**−**3**, **2**$^-$, **3**$^-$, and transition structures connecting them (ASCII); Tables 1S and 2S with the total energies, zero-point energies, and imaginary frequencies for the transition structures; Figure 1S with plots of activation energies vs frontier orbital energies. This material is available free of charge via the Internet at http://pubs.acs.org.

References and Notes

(1) Pillai, V. N. R. *Synthesis* **1980**, 1−26 and references therein.

(2) Barltrop, J. A.; Plant, P. J.; Schofield, P. *J. Chem. Soc., Chem. Commun.* **1966**, 822−823.

(3) (a) Patchornik, A.; Amit, B.; Woodward, R. B. *J. Am. Chem. Soc.* **1970**, *92*, 6333−6335. (b) Zehavi, U.; Amit, B.; Patchornik, A. *J. Org. Chem.* **1972**, *37*, 2281−2285.

(4) (a) Hébert, J.; Gravel, D. *Can. J. Chem.* **1974**, *52*, 187−189. (b) Gravel, D.; Murray, S.; Ladouceur, G. *J. Chem. Soc., Chem. Commun.* **1985**, 1828−1829.

(5) (a) Rich, D. H.; Gurwara, S. K. *J. Am. Chem. Soc.* **1975**, *97*, 1575−1579. (b) Rodebaugh, R.; Fraser-Reid, B.; Geysen, H. M. *Tetrahedron Lett.* **1997**, *38*, 7653−7656. (c) Whitehouse, D. L., Savinov, S. N.; Austin, D. J. *Tetrahedron Lett.* **1997**, *38*, 7851−7652.

(6) Beecher, J. E.; Cameron, J. F.; Fréchet, J. M. J. *J. Mater. Chem.* **1992**, *2*, 811−816 and references therein.

(7) (a) Kubota, S.; Tanaka, Y.; Moriwaki, T.; Eto, S. *J. Electrochem. Soc.* **1991**, *138*, 1080−1084. (b) Houlihan, F. M.; Nalamasu, O.; Kometani, J. M.; Reichmanis, E. *J. Imaging Sci. Technol.* **1997**, *41*, 35−40.

(8) Kaplan, J. H.; Forbush, B.; Hoffman, J. F. *Biochemistry* **1978**, *17*, 1929−1935.

(9) For reviews, see: *Methods Enzymol.* **1998**, *291*, 1−259 and references therein.

(10) Pelliccioli, A. P.; Wirz, J. *Photochem. Photobiol.* **2002**, *1*, 441−458 and references therein.

(11) (a) Lester, H. A.; Nerbonne, J. M. *Annu. Rev. Biophys. Bioeng.* **1982**, *11*, 151−175. (b) Gurney, A. M.; Lester, H. A. *Physiol. Rev.* **1987**, *67*, 583−617.

(12) (a) McCray, J. A.; Herbette, L.; Kihara, T.; Trentham, D. R. *Proc. Natl. Acad. Sci. U. S. A.* **1980**, *77*, 7237−7241. (b) Walker, J. W.; Reid, G. P.; McCray, J. A.; Trentham, D. R. *J. Am. Chem. Soc.* **1988**, *110*, 7170−7177. (c) Barth, A.; Hauser, K.; Maentele, W.; Corrie, J. E. T.; Trentham, D. R. *J. Am. Chem. Soc.* **1995**, *117*, 10311−10316. (d) Barth, A.; Corrie, J. E. T.; Gradwell, M. J.; Maeda, Y.; Maentele, W.; Meier, T.; Trentham, D. R. *J. Am. Chem. Soc.* **1997**, *119*, 4149−4159.

(13) McCray, J. A.; Trentham, D. R. *Annu. Rev. Biophys. Biophys. Chem.* **1989**, *18*, 239−270.

(14) Adams, S. R.; Tsien, R. Y. *Annu. Rev. Physiol.* **1993**, *55*, 755−784.

(15) (a) Walker, J. W.; Martin, H.; Schmitt, F. R.; Barsotti, R. J. *Biochemistry* **1993**, *32*, 1338−1345. (b) Marriott, G.; Heidecker, M. *Biochemistry* **1996**, *35*, 3170−3174. (c) Pan, P.; Bayley, H. *FEBS Lett.* **1997**, *405*, 81−85. (d) Cohen, B. E.; Stoddard, B. L.; Koshland, D. E., Jr. *Biochemistry* **1997**, *36*, 9035−9044. (e) Rossi, F. M.; Margulis, M.; Tang, C.-M.; Kao, J. P. Y. *J. Biol. Chem.* **1997**, *272*, 32933−32939. (f) Chaulk, S. G.; MacMillan, A. M. *Nucleic Acid Res.* **1998**, *26*, 3173−3178. (g) Papageorgiou, G.; Ogden, D. C.; Barth, A.; Corrie, J. E. T. *J. Am. Chem. Soc.* **1999**, *121*, 6503−6504.

(16) (a) Walker, J. W.; McCray, J. A.; Hess, G. P. *Biochemistry* **1986**, *25*, 1799−1805. (b) Milburn, T.; Matsubara, N.; Billington, A. P.; Udgaonkar, J. B.; Walker, J. W.; Carpenter, B. K.; Webb, W. W.; Marque, J.; Denk, W.; McCray, J. A.; Hess, G. P. *Biochemistry* **1989**, *28*, 49−55. (c) Billington, A. P.; Walstrom, K. M.; Ramesh, D.; Guzikowski, A. P.; Carpenter, B. K.; Hess, G. P. *Biochemistry* **1992**, *31*, 5500−5507. (d) Ramesh, D.; Wieboldt, R.; Billington, A. P.; Carpenter, B. K.; Hess, G. P. *J. Org. Chem.* **1993**, *58*, 4599−4605. (e) Gee, K. R.; Wieboldt, R.; Hess, G. P. *J. Am. Chem. Soc.* **1994**, *116*, 8366−8367. (f) Niu, L.; Gee, K. R.; Schaper, K.; Hess, G. P. *Biochemistry* **1996**, *35*, 2030−2036.

(17) Il'ichev, Yu. V.; Wirz, J. *J. Phys. Chem. A* **2000**, 104, 7856−7870.

(18) Il'ichev, Yu. V.; Schwörer, M.; Wirz, J. Submitted to *J. Am. Chem. Soc.*

(19) Il'ichev, Yu. V.; Kombarova, S. V.; Mac, M.; Schwörer, M.; Wirz, J. Unpublished results.

(20) Schwörer, M.; Wirz, J. *Helv. Chim. Acta* **2001**, *84*, 1441−1458.

(21) (a) Schupp, H.; Wong, W. K.; Schnabel, W. *J. Photochem.* **1987**, *36*, 85−97. (b) Zhu, Q. Q.; Schnabel, W.; Schupp, H. *J. Photochem.* **1987**, *39*, 317−332. (c) Wong, W. K.; Schupp, H.; Schnabel, W. *Macromolecules* **1989**, *22*, 2176−2181. (d) Schneider, S.; Fink, M.; Bug, R.; Schupp, H. *J. Photochem. Photobiol., A* **1991**, *55*, 329−338.

(22) Walbert, S.; Pfleiderer, W.; Steiner, U. *Helv. Chim. Acta* **2001**, *84*, 1601−1611.

(23) Cummings, R.; Krafft, G. A. *Tetrahedron Lett.* **1988**, *29*, 65−68. (b) Cummings, R.; DiZio, J. P.; Krafft, G. A. *Tetrahedron Lett.* **1988**, *29*, 69−72. (c) Krafft, G. A.; Sutton, W. R.; Cummings, R. *J. Am. Chem. Soc.* **1988**, *110*, 301−303.

(24) (a) Adams, S. R.; Kao, J. P. Y.; Grynkiewicz, G.; Minta, A.; Tsien, R. Y. *J. Am. Chem. Soc.* **1988**, *110*, 3212−3220. (b) Adams, S. R.; Kao, J. P. Y.; Tsien, R. Y. *J. Am. Chem. Soc.* **1989**, *111*, 7957−7968.

(25) (a) McCray, J. A.; Fidler-Lim, N.; Ellis-Davies, G. C. R.; Kaplan, J. H. *Biochemistry* **1992**, *31*, 8856−8861. (b) Ellis-Davies, G. C. R.; Kaplan, J. H. *Proc. Natl. Acad. Sci. U. S. A.* **1994**, *91*, 187−191.

(26) Muralidharan, S. Nerbonne, J. M. *J. Photochem. Photobiol., B* **1995**, *27*, 123−137.

(27) Frisch, M. J.; Trucks, G. W.; Schlegel, H. B.; Scuseria, G. E.; Robb, M. A.; Cheeseman, J. R.; Zakrzewski, V. G.; Montgomery, J. A., Jr.; Stratmann, R. E.; Burant, J. C.; Dapprich, S.; Millam, J. M.; Daniels, A. D.; Kudin, K. N.; Strain, M. C.; Farkas, O.; Tomasi, J.; Barone, V.; Cossi, M.; Cammi, R.; Mennucci, B.; Pomelli, C.; Adamo, C.; Clifford, S.; Ochterski, J.; Petersson, G. A.; Ayala, P. Y.; Cui, Q.; Morokuma, K.; Malick, D. K.; Rabuck, A. D.; Raghavachari, K.; Foresman, J. B.; Cioslowski, J.; Ortiz, J. V.; Stefanov, B. B.; Liu, G.; Liashenko, A.; Piskorz, P.; Komaromi, I.; Gomperts, R.; Martin, R. L.; Fox, D. J.; Keith, T.; Al-Laham, M. A.; Peng, C. Y.; Nanayakkara, A.; Gonzalez, C.; Challacombe, M.; Gill, P. M. W.; Johnson, B. G.; Chen, W.; Wong, M. W.; Andres, J. L.; Head-Gordon, M.; Replogle, E. S.; Pople, J. A. *Gaussian 98*, revision A.11; Gaussian, Inc.: Pittsburgh, PA, 1998.

(28) Spitznagel, G. W.; Clark, T.; Schleyer, P. v. R.; Hehre, W. J. *J. Comput. Chem.* **1987**, *8*, 1109−1116.

(29) Becke, A. D. *J. Chem. Phys.* **1993**, *98*, 5648−5652.

(30) (a) Lee, C.; Yang, W.; Parr, R. G. *Phys. Rev. B* **1988**, *37*, 785−797. (b) Stephens, P. J.; Devlin, F. J.; Chabalowski, C. F.; Frisch, M. J. *J. Phys. Chem.* **1994**, *98*, 11623−11627.

(31) (a) Perdew, J. P.; Wang, Y. *Phys. Rev.* **1992**, *B45*, 13244−13255. (b) Perdew, J. P.; Chavary, J. A.; Vosko, S. H.; Jackson, K. A.; Pederson, M. R.; Singh, D. J.; Fiolhais, C. *Phys. Rev.* **1992**, *B46*, 6671−6679.

(32) Becke, A. D. *J. Chem. Phys.* **1996**, *104*, 1040−1046. (b) Adamo, C.; Barone, V. *Chem. Phys. Lett.* **1997**, *274*, 242−250.

(33) Becke, A. D. *J. Chem. Phys.* **1993**, *98*, 1372−1377.

(34) (a) Miertus, S.; Scrocco, E.; Tomasi, J. *Chem. Phys.* **1981**, *55*, 117−129. (b) Miertus, S.; Tomasi, J. *Chem. Phys.* **1982**, *65*, 239−245. (c) Cossi, M.; Barone, V.; Cammi, R.; Tomasi, J. *Chem. Phys. Lett.* **1996**, *255*, 327−335.

(35) Peng, C.; Schlegel, H. B. *Isr. J. Chem.* **1993**, *33*, 449−454.

(36) (a) Fukui, K. *Acc. Chem. Res.* **1981**, *14*, 363−368. (b) Gonzalez, C.; Schlegel, H. B. *J. Phys. Chem.* **1990**, *94*, 5523−5527.

(37) Riddel, F. G. *Tetrahedron* **1981**, *37*, 849−858.

(38) (a) Brown, H. C.; Okamoto Y. *J. Am. Chem. Soc.* **1958**, *80*, 4979−4987. (b) Hansch, C.; Leo, A.; Taft, R. W. *Chem. Rev.* **1991**, *91*, 165−195.

(39) Shishkov, I. F.; Vilkov, L. V.; Kovács, A.; Hargittai, I. *J. Mol. Struct.* **1998**, *445*, 259−268.

(40) (a) Yip, R. W.; Sharma, D. K.; Giasson, R.; Gravel, D. *J. Phys. Chem.* **1984**, *88*, 5770−5772. (b) Gravel, D.; Giasson, R.; Blanchet, D.; Yip, R. W.; Sharma, D. K. *Can. J. Chem.* **1991**, *69*, 1193−1200.

(41) (a) Wang, X.-C.; Nichols, J.; Feyereisen, M.; Gutowski, M.; Boatz, J., Haymet, A. D. J.; Simons, J. *J. Phys. Chem.* **1991**, *95*, 10419−10424. (b) Zhang, Q.; Bell, R.; Truong, T. N. *J. Phys. Chem.* **1995**, *99*, 592−599. (c) Bell, R. L.; Taveras, D. L.; Truong, T. N.; Simons, J. *Int. J. Quantum Chem.* **1997**, *63*, 861−874. (d) Gu, J.; Leszczynski, J. *J. Phys. Chem. A* **1999**, *103*, 2744−2750.

(42) Tufariello, J. J. In *1,3-Dipolar Cycloaddition Chemistry*; Padwa, A., Ed.; Wiley: New York, 1984; Vol. 2, pp 83−168.

(43) Breuer, E.; Aurich, H. G.; Nielsen, A. In *Nitrones, nitronates, and nitroxides*; Patai, S., Rappoport, Z., Eds., Wiley: New York, 1989; pp 245−312.

(44) Carruthers, W. *Cycloaddition reactions in organic synthesis*; Pergamon Press: Oxford, 1990.

(45) For earlier work, see: (a) McDouall, J. J. W.; Robb, M. A.; Niazi, U.; Bernardi, F.; Schlegel H. B. *J. Am. Chem. Soc.* **1987**, *109*, 4642−4648 (b) Bernardi, F.; Bottoni, A.; Olivucci, M.; McDouall J. J. W.; Robb, M. A.; Tonachini, G. *THEOCHEM* **1988**, *42*, 341−351 and references therein.

(46) For recent publications, see: (a) Magnuson, E. C.; Pranata, J. *J. Comput. Chem.* **1998**, 19, 1795−1804. (b) Cossio, F. P.; Morao, I.; Jiao, H.; Schleyer, P. v. R. *J. Am. Chem. Soc.* **1999**, *121*, 6737−6746. (c) Di Valentin, C.; Freccero, M.; Gandolfi, R.; Rastelli, A. *J. Org. Chem.* **2000**, *65*, 6112−6120 and references therein.

(47) (a) Stowasser, R.; Hoffmann, R. *J. Am. Chem. Soc.* **1999**, *121*, 3414−3420 and references therein. (b) Hesselmann, A.; Jansen, G. *J. Chem. Phys.* **2000**, *112*, 6949−6952. (c) Lindgren, I.; Salomonson, S. *Int. J. Quantum Chem.* **2002**, *90*, 294−308.